
This manuscript has been accepted for publication in the *Journal of Nuclear Materials*. Please note that, despite having undergone peer-review, the manuscript has yet to be formally published. Printed version may have slightly different content. The final version of this manuscript will be available via the ‘Peer-reviewed Publication DOI’ link. Please feel free to contact the corresponding author. Any feedback will be greatly appreciated.

1 **Effect of solution chemistry on the iodine release from iodoapatite in aqueous environments**

2 Zelong Zhang ^{†*}, Léa Gustin^{‡1}, Weiwei Xie[‡], Jie Lian[§], Kalliat T. Valsaraj^{||}, and Jianwei Wang^{†,⊥}

3 [†] Department of Geology and Geophysics, Louisiana State University, Baton Rouge, Louisiana
4 70803 United States

5 [‡] Department of Chemistry, Louisiana State University, Baton Rouge, Louisiana 70803 United
6 States

7 [§] Department of Mechanical, Aerospace, and Nuclear Engineering, Rensselaer Polytechnic
8 Institute, 110 Eighth Street, Troy, New York 12180, United States

9 ^{||} Cain Department of Chemical Engineering, Louisiana State University, Baton Rouge,
10 Louisiana 70803 United States

11 [⊥] Center for Computation and Technology, Louisiana State University, Baton Rouge, Louisiana
12 70803, United States

13 *Corresponding to zelongz@lsu.edu

14

¹ Current address: Department of Chemistry, University of Wisconsin-Madison, Madison, Wisconsin 53706, United States

15 **Highlights**

- 16 • First study on the effect of aqueous ions on the degradation of waste form for I-129
- 17 • First summary on probable iodine release pathways in various aqueous environments
- 18 • Enhanced iodine release by enhanced ion-exchange, basic pH, and ionic strength.
- 19 • Discovered secondary phase vanadinite $Pb_5(VO_4)_3Cl$ and hydroxylvanadinite
- 20 $Pb_5(VO_4)_3OH$
- 21 • Low ionic content and neutral pH are vital to the disposal safety of nuclear waste

22

23 **Abstract**

24 To ensure the safe disposal of nuclear waste, understanding the release process of radionuclides
25 retained in the nuclear waste forms is of vital importance. Iodoapatite $\text{Pb}_{9.85}(\text{VO}_4)_6\text{I}_{1.7}$, a potential
26 waste form for iodine-129, was selected as a model system for ceramic waste forms in this study
27 to understand the effect of aqueous species on iodine release. Semi-dynamic leaching tests were
28 conducted on bulk samples in cap-sealed Teflon vessels with 0.1 mol/L NaCl, Na_2CO_3 , Na_3PO_4 ,
29 and Na_2SO_4 solutions under 90 °C, fixed sample surface area to solution volume ratio of 5/m,
30 and periodic replacement of leaching solutions. The reacted solutions were then analyzed by
31 Inductively Coupled Plasma-Mass Spectrometry and Inductively Coupled Plasma-Optical
32 Emission Spectrometry; the leached surfaces were characterized by X-ray diffraction, scanning
33 electron microscopy, and infrared spectroscopy. The result shows that, compared to deionized
34 water, the ion-rich solutions enhanced the iodine release as a result of the increased ionic
35 strength, reduced activity coefficient of dissolved species, and increased solution pH. Surface
36 reactions can lead to the formations of secondary phases by ion-exchange and precipitation.
37 These findings suggest that an ion-rich environment in the geological repository can be
38 detrimental to the disposal safety of the nuclear waste form.

39 **1 Introduction**

40 Nuclear energy is emission-free. The deployment of nuclear energy is motivated by the
41 pressing demand to mitigate climate change.¹ Sustainable development of the nuclear energy
42 requires concrete plans to safely dispose radionuclides waste generated by nuclear fission.²
43 Among those radionuclides, iodine-129 is particularly challenging to handle due to its long half-
44 life (15.7 million years), high yield (0.7% yield per fission of uranium-235),³ and weak
45 interactions with common materials in repository environments such as engineering barrier and
46 rock in geology formation.^{4,5} Iodide (I^-) is the most stable form of iodine in an environment with
47 pH and redox potential typically found in nature.⁶⁻⁸ Under highly oxidizing conditions, iodide
48 can be oxidized to iodine (I_2) and/or iodate (IO_3^-). All these iodine species are highly mobile in
49 nature given their high volatility and or high solubility.^{9,10} Iodine, as an essential element for
50 human health, can accumulate in human bodies.¹¹ For a healthy adult, 30% of the total iodine,
51 approximately 15-20 mg, is concentrated in the thyroid gland.¹² Chronical radiation from iodine-
52 129 beta decay can induce cancer to the thyroid follicular cells.¹¹ Therefore, iodine-129 is a
53 primary contributor of the radiation dosage when analyzing the safety of disposal environments.⁴
54 The immobilization of iodine-129 is one of the critical research subjects for nuclear waste
55 management.^{4,13-18}

56 The most probable scenarios that compromise nuclear waste forms in a repository
57 environment are the contact with aqueous solutions.^{19,20} In a typical repository, nuclear waste
58 forms are packed into corrosion resistant metallic canisters underground.²¹ Canister corrosion
59 and degradation are anticipated to be the result of corrodents carried by groundwater.²² Through
60 infiltration and percolation of precipitation and groundwater aquifer, water can reach the
61 canisters and supply corrodents to react with the canister material. Upon the breaching of the

62 canister, the waste forms are exposed to an aqueous environment. Owing to the long half-life of
63 iodine-129, it is crucial to predict the long-term chemical durability of iodine waste forms. To
64 enable such prediction, it is necessary to obtain a fundamental understanding of corrosion
65 mechanisms of waste forms and how iodine in the host material is released in various solutions
66 that may occur under repository conditions.

67 Several waste form materials including glass, ceramics, glass-ceramics, cement, and
68 composite have been proposed to immobilize iodine.^{18,23} These waste forms immobilize iodine
69 via two major mechanisms: encapsulation and incorporation. To encapsulate iodine, the host
70 matrices need to contain iodine in a designated phase different from the host material. One
71 example is zeolite structure, in which iodine-bearing phases can be adsorbed on zeolite's
72 framework.^{17,24} Iodine can also be incorporated as a compositional element into the host matrix
73 structure through chemical bonding, such as iodoapatite $Pb_5(VO_4)_3I$ and sodalite
74 $Na_4(AlSiO_4)_3I$.^{13,25-27}

75 The difficulty to study the durability of different waste forms varies on a case-by-case basis.
76 It is particularly challenging to evaluate the encapsulation waste forms due to the complexity of
77 multi-phase and microstructures. On the other hand, characterizing the corrosion mechanism can
78 be relatively straightforward for single-phase crystal waste forms which have well-defined
79 crystal structures and simple microstructures. Based on the simplicity of its crystal structure and
80 microstructure, iodoapatite is chosen in this study as the model system of ceramic waste forms
81 that can incorporate radionuclides. In addition, apatite ceramics is a promising material due to its
82 thermal, mechanical, and chemical stability.^{13,25,28,29} These advantages are also demonstrated in
83 nature as apatite has been found as a retention matrix for actinides and fission products in natural
84 fission reactors at Franceville basin in Africa.^{22,30}

85 Several chemical durability tests have been performed on single-phase crystal waste forms.
86 Uno et al. in 2001 conducted soxhlet leach method on apatite $\text{Pb}_{10}(\text{VO}_4)_6\text{I}_2$.³¹ Soxhlet leach
87 method is designed to maximize the number of leachable constituents in leachant by allowing a
88 continuous contact between the waste and recycling leachant in a closed system.³² The iodine
89 release rate, $3.98 \times 10^{-5} \text{ g} \cdot \text{cm}^{-2} \cdot \text{d}^{-1}$, was reported.³¹ Guy et al. in 2002 studied apatite
90 $\text{Pb}_{10}(\text{VO}_4)_{4.8}(\text{PO}_4)_{1.2}\text{I}_2$ dissolution in aqueous solutions.³³ The resulting data shows that iodine
91 release was incongruent and exhibited dependency on temperature and pH. They also discovered
92 a secondary phase, lead vanado-phosphate, precipitated at the sample surface. Zhang et al. in
93 2007 performed static leaching test on $\text{Pb}_5(\text{VO}_4)_3\text{I}$ powder in a basic KOH/KHCO_3 buffer
94 solution.³⁴ Spectroscopic evidences show that OH^- and CO_3^{2-} can substitute I^- and VO_4^{3-} in
95 apatite. Maddrell et al. in 2014 conducted static leach tests on crushed powder iodide sodalite
96 $\text{Na}_4(\text{AlSiO}_4)_3\text{I}$ in KOH/KHCO_3 buffer solutions.²⁶ The result suggests a congruent dissolution.²⁶
97 Three leaching static experiments with durations of 3, 7, and 14 days exhibited a logarithmic
98 increase of iodine release. More recently, in 2017 Coulon et al. applied static leaching technique
99 to study the iodate-substituted hydroxyapatite in deionized water and groundwater.³⁵ They
100 reported that the iodine release is controlled by congruent dissolution under unsaturated
101 conditions and controlled by diffusion through ion exchange under saturated condition.
102 Interestingly, when groundwater was used as leachant, secondary phase hydroxyapatite
103 precipitated on the sample surface. Based on these studies, static leach test is a preferable method
104 to study the waste form durability due to the following reasons: 1) its simple procedure can
105 accommodate a wide range of test conditions; 2) the resultant data can be used to interpret the
106 release mechanism.³⁶ Static leaching method assumes that the solution feedback is negligible,
107 which is valid under conditions of sufficiently low surface to volume ratio.³⁶ However, the

108 solution feedback can gradually increase over time in a static leaching experiment. In cases
109 where the solution is oversaturated for phases of low solubility, secondary phases can precipitate
110 at the leached surface. Therefore, it can be problematic to use data from static leaching tests to
111 predict waste form behavior in a repository environment.³⁷ To address the issues of solution
112 feedback, a semi-dynamic leaching method was implemented by Zhang et al. in 2018 to quantify
113 the processes involved in the iodine release of an iodine-bearing apatite.²⁹ In their experiment,
114 deionized water solutions, as the leachant, were replaced periodically to minimize the solution
115 feedback. They demonstrated that iodine released from apatite is driven by short-term diffusion
116 and long-term matrix dissolution. This semi-dynamic approach was employed to produce
117 essential datasets to parameterize a mechanistic model suitable for predicting the kinetics of
118 iodine release under different conditions.³⁷

119 Since the aqueous systems in natural environment contain a variety of dissolved species, it is
120 necessary to understand how these aqueous species affect the iodine release from iodine waste
121 forms in an aqueous environment. For instance, the iodine release from apatite structured
122 materials can be enhanced by rapid substitution of halogen element³⁸⁻⁴¹ or inhibited by
123 precipitation of secondary phase.^{33,35,37} In this study, we conducted semi-dynamic leach tests on
124 single phase crystal ceramics of iodoapatite in 0.1 mol/L NaCl, Na₂CO₃, Na₃PO₄ and Na₂SO₄
125 solutions. The goal is to examine the impact of the solution chemistry on the kinetics of
126 iodoapatite dissolution. We hypothesized that dissolved aqueous species, via ion exchange and
127 precipitation, can substantially impact the dissolution kinetics; this effect should highly depend
128 on the chemistry of the aqueous species and the surface reactions of specific phases. The finding
129 of this study is expected to provide important insight into the long-term performance of iodine
130 waste forms and guidance to improve the disposal safety of nuclear waste.

131 **2 Experimental**

132 **2.1 Materials and methods**

133 Our samples, obtained from previous studies,²⁵ were dense ceramic chips in
134 quadrilateral shape: 4.7 – 10.3 millimeter long by 1.1 – 1.8 millimeter thick with a
135 chemical composition of $\text{Pb}_{9.85}(\text{VO}_4)_6\text{I}_{1.7}$ according to the EDS and X-ray diffraction
136 refinement, as shown in Figs. 1, 2 and 4. The iodoapatite samples were synthesized by
137 using high energy ball milling (HEBM) and spark plasma sintering (SPS) techniques.
138 Sample surfaces were polished by 4000-grit sandpaper on a mechanical polishing wheel
139 lubricated with ethanol. Details of the synthesis and characterization of these samples
140 were reported previously in separate publications.^{25,29,37}

141 The leaching method was adopted from ASTM C1308 standard test, as described in
142 the previous study^{29,37}. Four parallel experiments were conducted simultaneously for 14
143 days in four different leaching solutions: 0.1 mol/L NaCl, 0.1 mol/L Na_2CO_3 , 0.1 mol/L
144 Na_3PO_4 , and 0.1 mol/L Na_2SO_4 . Sample surface area (m^2) to solution volume (m^3) ratios
145 (S/V) of all four tests were fixed and maintained at 5/m. The leached solutions were
146 replaced every 24 hours. All reactor vessels were weighed before and after each interval
147 to monitor the solution losses which were within 0.5 % of the initial solution mass. In
148 addition, a control test was conducted in deionized water under identical conditions for 7
149 days using the same protocol. All samples after leaching experiments were collected,
150 rinsed by deionized water and ethanol, and air-dried.

151 **2.2 Characterization**

152 The elements of interest in the leachate solutions are I, Pb, and V. The leached
153 solutions, depending on the solution chemistry, were analyzed by Inductively Coupled
154 Plasma-Mass Spectrometry (ICP-MS, PerkinElmer Elan 9000) and/or Inductively-
155 Coupled Plasma-Optical Emission Spectrometry (ICP-OES, SPECTRO Ametek Spectro
156 ARCOS). Two standard solutions from Inorganic Ventures were used in the solution
157 analysis: 1) $1.001 \pm 0.007 \mu\text{g}/\text{mL}$ iodide in H_2O solution and 2) $1.000 \pm 0.007 \mu\text{g}/\text{mL}$
158 lead and $1.000 \pm 0.006 \mu\text{g}/\text{mL}$ vanadium in 1% HNO_3 solution. Chemical properties of
159 solution at equilibrium state such as pH, ionic strength, speciation, and activity were
160 calculated by Visual MINTEQ package.

161 Samples were characterized by Scanning Electron Microscopy (SEM), Infrared
162 spectroscopy (IR), and X-ray diffraction spectroscopy (XRD). SEM images were taken by
163 a FEI Quanta SEM system with FEI Versa 3D DualBeam. Infrared spectroscopy was
164 performed on a Thermo Nicolet Continuum Infrared Microscope under Specular
165 Reflection mode and transmission mode with a fixed incident angle and an aperture area
166 of 10 by 10 μm covering 4000 to 650 cm^{-1} at a spectral resolution of 2 cm^{-1} . XRD data
167 were collected from PANalytical Empyrean X-Ray Diffractometer equipped with
168 monochromated $\text{Cu-K}\alpha$ radiation ($\lambda = 1.5406 \text{ \AA}$), operated at 45 kV, 40 mA, a step size of
169 0.026° , and a scanning range from 5 to 100° .

170 The crystal structures were refined by Le Bail algorithm using Jana2006 program.⁴²
171 All parameters were refined by the least-squares method. The pseudo-Voigt function was
172 used as the peak profile function. Structural parameters of $\text{Pb}_{9.85}(\text{VO}_4)_6\text{I}_{1.7}$ measured by
173 Audubert et al. were used as initial input (hexagonal, space group P63/m, $a = b = 10.422$
174 \AA , $c = 7.467 \text{ \AA}$, $\alpha = \beta = 90^\circ$; $\gamma = 120^\circ$).⁴³

175 **3 Results**

176 **3.1 Leached surface characterization by SEM/EDS**

177 In Fig. 1 (a-c), no changes observable by naked eyes occurred on the surfaces of
178 samples leached by NaCl and NaSO₄ solutions for 14 days, whereas white layers were
179 gradually formed on the sample surfaces leached by Na₂CO₃ and Na₃PO₄ solutions within
180 the first week of the experiments. The SEM images in Fig. 1 (d-i) show that the surface
181 alterations on samples leached by NaCl and Na₂SO₄ solutions were moderate, similar to
182 the water leached surface. However, samples leached by Na₂CO₃ and Na₃PO₄ solutions
183 demonstrated significant surface corrosion and possible formation of new phases. The
184 surface leached by Na₂CO₃ exhibited large grains, while congregated structures of similar
185 size appeared on the surface leached by Na₃PO₄.

186 According to EDS analysis, the surface chemical compositions in Fig. 2 indicate
187 considerable changes between the leached samples and the pristine one. The key features
188 of EDS spectrum of pristine iodoapatite are: a carbon peak at 0.3 keV from background
189 (carbon tape), an oxygen peak at 0.5 keV, a broad Pb band from 2.34 to 2.45 keV
190 shouldered with two small Pb peaks at 1.8 and 2.6 keV, three iodine peaks at 3.9, 4.2, and
191 4.5 keV, and vanadium peaks at 4.9 and 5.4 keV. Overall, the iodine peaks at 3.94 keV
192 are nearly diminished in the EDS spectra of all four leached surfaces. The samples
193 leached by NaCl and Na₃PO₄ exhibited a substantial amount of chloride and phosphorus
194 signals at 2.62 and 2.01 keV, respectively. On the sample leached by NaCl, the Pb peak at
195 2.62 keV is comparable to the Pb peak at 1.8 keV, while the 2.62 keV peaks of the rest
196 samples are much weaker than their corresponding 1.8 keV peaks. Carbon signal at 0.27

197 keV from Na₂CO₃ leached sample cannot be properly quantified due to the background
198 interference from carbon tape and the graphite impurity introduced during sample
199 synthesis. Sulfur EDS peak at 2.31 keV overlaps with the broad central peak of Pb at 2.34
200 keV. Na₂SO₄ leached surface exhibited no sulfur peak near 2.3 keV given the
201 resemblance of the band shape between the sample leached by Na₂SO₄ and the rest. We
202 noticed variations of carbon and oxygen EDS signals among these samples which were
203 induced by the instrumentation settings such as sample orientation and beam parameters.
204 Therefore, carbon and oxygen were not considered in the EDS analysis.

205 **3.2 Leached surface characterization by IR analysis**

206 The IR spectroscopy results are listed in Fig. 3. All these four samples yielded two
207 main peaks near 750 and 890 cm⁻¹, which are attributed to V-O bond.³⁴ Pristine
208 iodoapatite and samples leached by water, Na₂SO₄, and NaCl showed nearly identical
209 spectra. Surfaces leached by Na₂CO₃ and Na₃PO₄ exhibited position shifts of these two
210 V-O peaks to the region of 700 to 900 cm⁻¹ and multiple new bands. Sample leached by
211 Na₂CO₃ yielded sharp bands near 785, 890, 960, 1200, and 1450 cm⁻¹, in which the broad
212 band at 1450 cm⁻¹ is attributed to the stretching vibration of CO₃²⁻.^{44,45} The Na₃PO₄
213 leached surface generated IR peaks near 785, 870, 950, 1110, 1420, 1800, and 2200 cm⁻¹,
214 in which some can be assigned to the PO₄³⁻ (e.g. ν_1 – 950 cm⁻¹, ν_3 – 1100 cm⁻¹).⁴⁴
215 Interestingly, both CO₃²⁻ and PO₄³⁻ leached surfaces showed visible OH⁻ stretching
216 vibration near 3500 cm⁻¹,^{34,44} which also occurred on water leached surface under IR
217 transmission mode.²⁹

218 **3.3 Leached surface characterization by XRD**

219 The XRD data are shown in Fig. 4. All these leached samples demonstrated
220 substantial differences compared to the pristine sample. Based on the XRD pattern, these
221 leached samples can be categorized into two groups: I) surfaces leached by NaCl and
222 Na₂SO₄ solutions, the pristine, and water leached sample; II) surfaces leached by Na₂CO₃
223 and Na₃PO₄ solutions, which were similar to the standard hydroxylvanadinite. The XRD
224 patterns of Group I are alike, which indicates no substantial structural changes compared
225 to the pristine. The XRD patterns of Group II display enhanced peak splitting between
226 25° and 28°. The original peak splitting of the pristine sample reflects the apatite structure
227 deformation which accommodates the relatively large iodide incorporated in the apatite
228 framework. The peak splitting of Na₂SO₄ leached surface is slightly enhanced, compared
229 to the pristine, but is weaker than the water leached sample. Interestingly, NaCl leached
230 surface yielded a diminished splitting at 26° and a new peak occurred at 29°, later
231 identified as $1\bar{3}1$ shown in Fig. 5. The Full Width at Half Maximum (FWHM) of XRD
232 from NaCl leached surface was considerably broadened to ~0.4° compared to ~0.2° from
233 other samples, which may be attributed to the peak overlapping resulting from the
234 presence of a secondary phase. Both Na₂CO₃ and Na₃PO₄ leached samples exhibited
235 nearly identical XRD pattern, resembling the pattern of standard hydroxylvanadinite
236 Pb₁₀(VO₄)₆(OH)₂. The two highest bands on Pb₁₀(VO₄)₆(OH)₂ standard are 112 and $1\bar{3}1$
237 with an order of intensity $I_{112} < I_{1\bar{3}1}$. Same bands 112 and $1\bar{3}1$ also have the highest
238 intensity on Na₂CO₃ and Na₃PO₄ leached samples, however, the intensity of 112 is higher
239 than that of $1\bar{3}1$, $I_{112} > I_{1\bar{3}1}$.

240 The Le Bail method was applied to obtain structural information from the XRD data.
241 Table 1 compares the refined lattice parameters between sample surfaces of different

242 conditions and standards. No noticeable changes occurred in the crystal structures of
243 samples leached by deionized water and Na₂SO₄ when compared to that of pristine
244 sample (their length of *a*-, *b*-, and *c*-axes are approximately ~10.4, ~10.4, and ~7.5 Å,
245 respectively). On the other hand, a ~0.2 Å contraction along both the *a*- and *b*-axes were
246 observed for the samples leached by Na₂CO₃ and Na₃PO₄ solutions while the *c*-axis
247 remains the same and is consistent with other samples at ~7.45 Å. The observed and
248 calculated diffraction patterns, the residual and the indices of the main reflections of NaCl
249 leached sample are shown in Fig. 5. We identified a secondary phase vanadinite
250 Pb₅(VO₄)₃Cl, indicating the substitution of iodine by chlorine during NaCl leaching.

251 **3.4 Solution composition analysis by ICP-MS and ICP-OES**

252 The results of the solution analysis on the leachates collected from the leach tests are
253 shown in Fig. 6. The release rates of iodine, lead, and vanadium are depicted as green
254 circles, blue squares, and red triangles, respectively. In Fig. 6(a), iodine release in NaCl
255 solution gradually increased over time, reaching a maximum rate near 0.8 mmol/m²/d at
256 day 11, and then slightly decreased near the end of the 14-day test. The Pb and V release
257 exhibited similar patterns with a relatively high initial rate around 0.075 mmol/m²/d, then
258 gradually decreased, and eventually approached a plateau near 0.05 mmol/m²/d. In Fig.
259 6(b), the release patterns of iodine and vanadium in Na₂CO₃ are similar: release rates
260 rapidly reached maximum near day 2 and then gradually decreased over time approaching
261 a plateau. However, the long-term rate of Pb in Na₂CO₃ appears to be constant. In Fig.
262 6(c), the iodine release in Na₂SO₄ exhibited a high initial rate approximately 0.32
263 mmol/m²/d and then its rate gradually decreased, eventually approaching a plateau around
264 0.15 mmol/m²/d. Despite no high initial release, the Pb and V release patterns follow the

265 trend of iodine release: gradually decreased over time and then rebounded near day 10.
266 The Fig. 6(d) describes the element release of iodoapatite in Na_3PO_4 , which shows
267 constant rates of ~ 4.5 , ~ 3.5 , and ~ 13 $\text{mmol/m}^2/\text{d}$ for the release for iodine, Pb, and V,
268 respectively. Due to the instrumentation limitation and sample consumption, only four
269 leachates from the Na_3PO_4 experiment was analyzed for their Pb content.

270 Leaching rates of I, Pb, and V based on the solutions analysis are compared in Figs.
271 7(a-c), respectively. In general, leaching tests conducted in the ionic solutions present
272 significantly higher element release rates than those of deionized water in the order of
273 $\text{Na}_3\text{PO}_4 > \text{Na}_2\text{CO}_3 > \text{Na}_2\text{SO}_4 > \text{water}$, except in the NaCl solution. In Fig. 7(a), iodine
274 release from Na_3PO_4 , Na_2CO_3 , and Na_2SO_4 solutions exhibited a long-term leach pattern
275 similar to that of water leaching: started with a high initial release, then gradually
276 decreased, and eventually stabilized and reached a plateau. The iodine release in NaCl
277 solution, however, presents a different pattern: iodine rate increased from the beginning
278 of leach test to day 11, when the rate reached maximum and then stabilized. The release
279 rates of Pb and V from NaCl test are relatively constant but not higher than those of water
280 leached as shown in Figs. 7(b, c).

281 The molar ratios in leachate solutions are illustrated in Figs. 7(d, e). Except for the
282 anomalous NaCl data, the long-term I/V ratios in Fig. 7(d) fluctuate around the ratio of
283 water-leached sample within the range of [0.34, 1.02], which are higher than the
284 stoichiometric value 0.28. In Fig. 7(e), the long-term Pb/V ratios of NaCl and Na_2SO_4
285 tests are 1.36 and 1.65, approximate to the stoichiometric value 1.64, whereas the long-
286 term ratios from Na_2CO_3 and Na_3PO_4 tests are 0.95 and 0.27, significantly lower than
287 1.64.

288 **3.5 Overview of leaching rates in solutions**

289 The phases of interest in this study are the aqueous solutions and the solid surfaces.
290 The leachate solution chemistry in Fig. 7 shows that iodine release from the sample
291 leached by the NaCl solution has a distinctive pattern. For the other leach tests, the long-
292 term iodine rates (plateau region in Figs. 6-7) are at least one magnitude higher than that
293 from water leaching. And the order of iodine leach rate, based on solution analysis in Fig
294 7 (a), is consistent with the orders of Pb and V rates in Fig. 7 (b, c): $R_{\text{Pb/V/I}}(\text{Na}_3\text{PO}_4) >$
295 $R_{\text{Pb/V/I}}(\text{Na}_2\text{CO}_3) > R_{\text{Pb/V/I}}(\text{Na}_2\text{SO}_4) > R_{\text{Pb/V/I}}(\text{deionized water})$. In the following section,
296 we will analyze the anomalous result of NaCl leach test and then explain how element
297 release behaviors differentiate due to the different solution chemistry, such as pH and
298 ionic species.

299 **4 Discussion**

300 **4.1 Anomaly of the sample leached by NaCl solution**

301 Iodoapatite sample leached by 0.1 mol/L NaCl solution exhibited unique surface
302 phase composition and iodine release pattern. The XRD data in Figs. 4 and 5 show
303 leached surface has no apparent splitting in the region from 25° to 28° (2θ) and a new
304 peak ($\bar{1}\bar{3}1$), attributed by a vanadinite phase. This anomaly suggests a reduced structural
305 distortion, which can be contributed by substituting iodide with smaller chloride. The
306 refinement in Fig. 5 confirmed new phase vanadinite was formed on the surface, which
307 resembles the XRD pattern of iodoapatite $\text{Pb}_{9.85}(\text{VO}_4)_6\text{I}_{1.7}$. The XRD data is consistent
308 with the EDS result and solution analysis. The Pb EDS band at 2.6 keV, in Fig 2, is
309 comparatively enhanced due to the overlap by chlorine signal at 2.6 keV. The release

310 rates of iodine from the NaCl test in Fig. 6(a) suggest the new phase was growing until
311 the equilibrium state was reached. A similar iodine release pattern was observed in a pH 4
312 semi-dynamic leaching experiment, of which the rate anomaly was caused by the
313 formation of a secondary phase.³⁷ The molar ratios of Pb/V in Fig. 7(e) approximate to
314 the stoichiometric value 1.6, indicating a congruent dissolution of Pb and V. The variation
315 of I/V molar ratios in Fig. 7(d) is consistent with that of iodine rates in Fig. 6(a). Both the
316 I/V ratios and iodine rates suggest an incongruent release for iodine, unlike the congruent
317 Pb and V. The SEM images in Figs. 1(b, e) show that both surfaces leached by NaCl and
318 deionized water share similar morphology. The new phase vanadinite $Pb_5(VO_4)_3Cl$,
319 confirmed by the XRD refinement, suggests ion-exchange process between iodide and
320 chloride. This postulation is supported by the solution and surface analysis that 1) a
321 significant amount of iodine was released into NaCl solution while the Pb and V rates are
322 comparable to the data of water leach test as shown in Figs. 6-7; 2) the surface alteration
323 revealed by SEM in Fig. 1 and the surface chemistry by EDS in Fig. 2 resemble those of
324 deionized water. Interestingly, the structural deformation of the original iodine-bearing
325 apatite $Pb_{9.85}(VO_4)_6I_{1.7}$ appeared to be restored in the chlorine-substituted structure
326 vanadinite $Pb_5(VO_4)_3Cl$. Given that the ionic radius of chloride (Cl^- , $1.68 \pm 0.19 \text{ \AA}$) is
327 considerably smaller than that of iodide (I^- , $2.11 \pm 0.19 \text{ \AA}$),⁴⁶ exchanging the iodide with
328 smaller chloride seems to have repaired the structural deformation.

329 **4.2 Effect of pH on iodine release and secondary phase formation**

330 The solution pH has a strong effect on the iodine release of the iodoapatite. Chemical
331 properties of the leaching solutions calculated by VMINTEQ are listed in Table 2.
332 According to our previous studies, iodoapatite dissolution in deionized water can be

333 represented by the congruent release of Pb and V.²⁹ In Fig. 7 (b, c), the Pb and V rates
334 from different solutions are generally constant, indicating a constant-dissolution
335 controlled process. The overall dissolution rates from low to high appears to be: R
336 (*deionized water*) < R (Na_2SO_4) < R (Na_2CO_3) < R (Na_3PO_4), which corresponds to the
337 solution pH values ~6.1, ~6.2, ~10.3, and ~10.9 under 90 °C as listed in Table 2.
338 Therefore, increasing pH from neutral to basic can increase the iodine release by
339 enhancing the overall dissolution of the iodoapatite, which is consistent with previous
340 experimental results on synthetic iodoapatite and natural apatites^{33,47}. However, due to the
341 secondary phase formed in Na_2CO_3 solutions, the dissolution process was being
342 continuously hindered by the accumulating precipitates. Interestingly, the trend of iodine
343 released in Na_2CO_3 solution of pH 10.3 resembles that of leaching iodoapatite under pH
344 4.³⁷ Despite the rate difference, both surfaces leached by pH 4 and pH 10.3 formed
345 secondary phases (chervetite and hydroxylvanadinite, respectively). Our previous study
346 showed that the equivalent long-term rate of iodine release under pH 6 is 8.1 mmol/m²/d,
347 over two magnitudes higher than that of the deionized water 0.036 mmol/m²/d.³⁷
348 Nevertheless, the release rates of iodine leached by the solutions of non-neutral pH are at
349 least one magnitude higher than that of the neutral pH solutions due to the enhanced
350 dissolution process.

351 Surface characterizations indicate the presence of new phases under the basic
352 conditions. The XRD analysis in Fig. 4 and Table 1 shows the surfaces leached by the
353 Na_2CO_3 and Na_3PO_4 solutions were dominated by secondary phases resembling
354 hydroxylvanadinite $Pb_{10}(VO_4)_6(OH)_2$. The SEM in Fig. 1 reveals different grain shapes
355 and sizes from the water leached, while the EDS in Fig. 2 demonstrates that iodine was

356 depleted on the surface. The solution analysis also supports the formation of new phase
357 given the similar element release pattern to that of pH 4 and incongruent Pb/V ratios far
358 away from the stoichiometric value. As shown in Fig. 7, the leaching rates of all elements
359 are at least one magnitude higher than the water leach rates of corresponding elements.
360 The results from this study and those from relevant literature suggest that the solution pH
361 exerts significant effects on the dissolution rate and the secondary phase formation in
362 aqueous environments such as chervetite and hydroxyvanadinite precipitated under acidic
363 and basic conditions, respectively.^{37,48,49}

364 **4.3 Effect of ionic species on the dissolution rate**

365 In this study, dissolved species affected the sample dissolution process by increasing
366 the ionic strength in solution, which consequently reduced the activity coefficient of
367 dissolved species. As a result, saturation state and solution feedback were reduced, which
368 in return increased the dissolution rate.⁴⁷ Although the 0.1 mol/L Na₂SO₄ and 0.1 mol/L
369 NaCl solutions have approximately the same solution pH as deionized water, the
370 dissolution rates in these ionic solutions are significantly higher than that of the deionized
371 water. As shown in Table 2, 0.1 mol/L Na₂SO₄ solution gives total ionic strength of 0.26
372 mol/L, 0.1 mol/L NaCl solution 0.098 mol/L, and deionized water 2.04×10^{-6} mol/L close
373 to zero. The vast difference in ionic strength leads to different degrees of saturation state.
374 The activity coefficient of the major ions Na⁺, Cl⁻, and SO₄²⁻ in these ionic solutions are
375 ranging from 0.25 to 0.76, considerably lower than the major ions H⁺ and OH⁻ with a
376 respective activity coefficient 1.00 in the deionized water. The dissolution rate in 0.1
377 mol/L Na₂SO₄ solution is higher than the rate in the 0.1 mol/L NaCl solution and
378 deionized water under the same pH and reaction mechanism, as shown in Fig. 7.

379 Moreover, the average release rate of iodine in Na₃PO₄ (pH 10.9) is about one magnitude
380 higher than that of Na₂CO₃ (pH 10.3) despite their similar pHs. The difference in rates can be
381 inferred from the difference in ionic strength: 0.29 mol/L for 0.1 mol/L Na₃PO₄ and 0.25
382 mol/L for Na₂CO₃ solution.

383 In addition, no substantial structure change happened to the sample leached by 0.1
384 mol/L Na₂SO₄ solution. It is unlikely that anion SO₄²⁻ can be incorporated into apatite
385 structure as there is no evidence from surface characterization and solution analysis to
386 support that. No structural change was detected by the XRD characterization. The SEM
387 images and EDS analysis in Figs. 1 and 2 show that the Na₂SO₄ and water leached
388 surfaces have a similar grain size, surface morphology, and chemical composition. The
389 element release rates and ratios in Fig. 7 and 8 demonstrate a similar leach behavior
390 between samples leached by Na₂SO₄ and deionized water. The similarities in surface
391 alteration and leaching behavior between samples leached by Na₂SO₄ and water suggest
392 that the iodine release in Na₂SO₄ solution was controlled by short-term diffusion and
393 long-term dissolution and the release of Pb and V is controlled by congruent dissolution.
394 No precipitated was observed on Na₂SO₄ leached surface, which is also similar to the
395 surface leached by water.

396 In terms of the surface precipitation, the SEM images in Figs. 1 (c, f) reflect intense
397 surface alterations in the solutions of Na₃PO₄ and Na₂CO₃. The leached surfaces yielded
398 XRD patterns similar to the standard hydroxyvanadinite Pb₅(VO₄)₃OH. However,
399 significant contractions of *a*- and *b*-axes as shown in Table 2 indicate the size of VO₄ site
400 was reduced, which could be caused by a substitution of smaller groups.⁵⁰ The IR
401 spectroscopy of the sample leached by Na₃PO₄ confirms the existence of P-O bond and

402 OH⁻. Furthermore, the EDS detected phosphorus signal, which also supports that PO₄
403 group was in VO₄ site. The molar ratios of Pb/V in Fig. 7 show a deficiency of Pb relative
404 to V in Na₃PO₄ leaching test. These evidences suggest the precipitates are a product of
405 hydroxyvanadinite with mixed site: Pb₁₀(VO₄)_n(PO₄)_{6-n}(OH)₂. The site mixing is possible
406 since Pb₁₀(VO₄)_x(PO₄)_{6-x}(OH)₂ can occur during wet chemistry reactions under similar
407 conditions.⁴⁸ Carbonate is known to be incorporated into apatite structure by
408 substitution.⁵⁰⁻⁵³ Given that phosphate (PO₄³⁻, ionic radius 2.30 ± 0.42 Å)⁴⁶ can replace
409 vanadate in iodoapatite,⁴⁸ it is reasonable to presume that carbonate of a smaller ionic
410 radius (CO₃²⁻, 1.89 ± 0.19 Å)⁴⁶ can substitute vanadate in a similar crystal structure.
411 Therefore, the secondary phase formed on in the Na₂CO₃ solution is Pb₁₀(VO₄)₆₋
412 _m(CO₃)_{1.5m}(OH)₂.

413 **4.4 Mechanism of iodoapatite dissolution and surface reactions in aqueous** 414 **environments**

415 Fig. 8 generalizes the mechanism of iodoapatite dissolutions with multiple processes
416 contributing to the iodine release. Our previous study on iodine release in deionized water
417 suggests that the iodine release is driven by short-term diffusion and long-term
418 dissolution.²⁹ Diffusion and dissolution are affected by various factors of the solution
419 chemistry, such as solution ionic strength, pH, and secondary phase formation resulted
420 from a supersaturation of the solution with respect to low solubility species. In neutral pH
421 solutions, the iodine release is subjected to the substitution of iodine by anionic species in
422 solution such as OH⁻ and Cl⁻. When dealing with solutions of comparable pH, a higher
423 ionic strength, due to the ionic content, can enhance the dissolution by changing
424 saturation conditions. Solution pH other than near neutral can increase the dissolution by

425 exponentially accelerating the dissolution process. The resulting rapid dissolution can
426 often lead to the precipitation of secondary phases when the solution approaches the
427 supersaturation state of low solubility phases. Possible secondary phases include
428 chervetite $\text{Pb}_2\text{V}_2\text{O}_7$ under acidic condition³⁷ and hydroxylvanadinite $\text{Pb}_5(\text{VO}_4)_3\text{OH}$ under
429 basic condition.

430 **5 Conclusions**

431 The present study focuses on effects by solution compositions on iodoapatite
432 dissolution. The results suggest that the higher ionic strength can accelerate dissolution by
433 decreasing the activity coefficient of reacting aqueous species, thus promoting iodine
434 release from apatite. Non-neutral pH conditions clearly increase the dissolution rate and
435 often lead to precipitations of secondary phases, such as chervetite and
436 hydroxylvanadinite. The secondary phase precipitation at the surfaces hinders the
437 dissolution rate by reducing the available reacting surface area. However, the overall
438 iodine release rates in both basic and acidic solutions are exponentially higher than those
439 in the near-neutral pH conditions, especially in deionized water. Current understanding of
440 dissolution is mostly based on leaching experiments conducted in deionized water. Our
441 investigation on the impact of solution chemistry reveals new complexities of the
442 dissolution kinetics of crystalline waste form during environmental degradation, Unlike
443 fresh water with low ion content, high concentrations of aqueous species commonly
444 found in underground brines can compromise the chemical durability of crystalline waste
445 form in a geological repository. For this specific waste form, maintaining neutral pH and
446 low ion content in aqueous solutions is important to the disposal safety of radioactive
447 iodine. Since iodine is one of the most challenging radionuclides to immobilize, building

448 a comprehensive theoretical framework of iodine immobilization can significantly
449 advance the research in nuclear waste disposal safety.

450 **Conflicts of interest**

451 There are no conflicts to declare.

452 **Acknowledgements**

453 This work was supported as part of the Center for Performance and Design of Nuclear
454 Waste Forms and Containers, an Energy Frontier Research Center funded by the U.S.
455 Department of Energy, Office of Science, Basic Energy Sciences (DE-SC0016584). The
456 sample surface characterizations were carried out at the Shared Instrumentation Facilities
457 (SIF) and Center for Advanced Microstructures and Devices (CAMD) of Louisiana State
458 University. We thank our XRD & Geochemistry Lab Researcher Wanda LeBlanc for
459 operating XRD experiments at SIF and facilitating our experiments in Geochemistry Lab.
460 We also thank Dr. Orhan Kizilkaya from CAMD for his assistance on infrared
461 spectroscopy.

462 **Date Availability**

463 Data will be made available on request

464 **References**

- 465 (1) Climate Change 2014: Mitigation of Climate Change: Working Group III Contribution to the Fifth
466 Assessment Report of the Intergovernmental Panel on Climate Change; Intergovernmental Panel
467 on Climate Change, Edenhofer, O., Eds.; Cambridge University Press: New York, NY, 2014.
- 468 (2) Alley, W. M.; Alley, R. The Growing Problem of Stranded Used Nuclear Fuel. *Environ. Sci. Technol.*
469 **2014**, 48 (4), 2091–2096. <https://doi.org/10.1021/es405114h>.
- 470 (3) Nichols, A. L.; Verpelli, M.; Aldama, D. L. Handbook of Nuclear Data for Safeguards; INDC(NDS)--
471 0502; International Atomic Energy Agency, 2007.
- 472 (4) Ojovan, M. I.; Lee, W. E. 10 - Long-Lived Waste Radionuclides. In *An Introduction to Nuclear
473 Waste Immobilisation (Second Edition)*; Ojovan, M. I., Lee, W. E., Eds.; Elsevier: Oxford, 2014; pp
474 107–115. <https://doi.org/10.1016/B978-0-08-099392-8.00010-3>.
- 475 (5) Aimoz, L.; Wieland, E.; Taviot-Guého, C.; Dähn, R.; Vespa, M.; Churakov, S. V. Structural Insight
476 into Iodide Uptake by AFm Phases. *Environ. Sci. Technol.* **2012**, 46 (7), 3874–3881.
477 <https://doi.org/10.1021/es204470e>.
- 478 (6) Um, W.; Serne, R. J.; Krupka, K. M. Linearity and Reversibility of Iodide Adsorption on Sediments
479 from Hanford, Washington under Water Saturated Conditions. *Water Res.* **2004**, 38 (8), 2009–
480 2016. <https://doi.org/10.1016/j.watres.2004.01.026>.
- 481 (7) Coughtrey, P. J.; Thorne, M. C. Radionuclide Distribution and Transport in Terrestrial and Aquatic
482 Ecosystems. *A Critical Review of Data*; 1983; Vol. 1.
- 483 (8) Whitehead, D. C. The Distribution and Transformations of Iodine in the Environment. *Environ. Int.*
484 **1984**, 10 (4), 321–339. [https://doi.org/10.1016/0160-4120\(84\)90139-9](https://doi.org/10.1016/0160-4120(84)90139-9).
- 485 (9) Schwehr, K. A.; Santschi, P. H.; Kaplan, D. I.; Yeager, C. M.; Brinkmeyer, R. Organo-Iodine
486 Formation in Soils and Aquifer Sediments at Ambient Concentrations. *Environ. Sci. Technol.* **2009**,
487 43 (19), 7258–7264. <https://doi.org/10.1021/es900795k>.
- 488 (10) Shimamoto, Y. S.; Takahashi, Y.; Terada, Y. Formation of Organic Iodine Supplied as Iodide in a
489 Soil–Water System in Chiba, Japan. *Environ. Sci. Technol.* **2011**, 45 (6), 2086–2092.
490 <https://doi.org/10.1021/es1032162>.
- 491 (11) Fuge, R.; Johnson, C. C. Iodine and Human Health, the Role of Environmental Geochemistry and
492 Diet, a Review. *Appl. Geochem.* **2015**, 63, 282–302.
493 <https://doi.org/10.1016/j.apgeochem.2015.09.013>.
- 494 (12) Patrick, L. Iodine: Deficiency and Therapeutic Considerations. *Altern. Med. Rev.* **2008**, 13 (2), 116–
495 127.
- 496 (13) Audubert, F.; Carpena, J.; Lacout, J. L.; Tetard, F. Elaboration of an Iodine-Bearing Apatite Iodine
497 Diffusion into a Pb₃(VO₄)₂ Matrix. *Solid State Ion.* **1997**, 95 (1), 113–119.
498 [https://doi.org/10.1016/S0167-2738\(96\)00570-X](https://doi.org/10.1016/S0167-2738(96)00570-X).
- 499 (14) Garino, T. J.; Nenoff, T. M.; Krumhansl, J. L.; Rademacher, D. X. Low-Temperature Sintering Bi–Si–
500 Zn-Oxide Glasses for Use in Either Glass Composite Materials or Core/Shell 129I Waste Forms. *J.*
501 *Am. Ceram. Soc.* **2011**, 94 (8), 2412–2419. <https://doi.org/10.1111/j.1551-2916.2011.04542.x>.
- 502 (15) Krumhansl, J. L.; Nenoff, T. M. Hydrotalcite-like Layered Bismuth–Iodine–Oxides as Waste Forms.
503 *Applied Geochemistry* **2011**, 26 (1), 57–64. <https://doi.org/10.1016/j.apgeochem.2010.11.003>.
- 504 (16) Sava, D. F.; Garino, T. J.; Nenoff, T. M. Iodine Confinement into Metal–Organic Frameworks
505 (MOFs): Low-Temperature Sintering Glasses To Form Novel Glass Composite Material (GCM)
506 Alternative Waste Forms. *Ind. Eng. Chem. Res.* **2012**, 51 (2), 614–620.
507 <https://doi.org/10.1021/ie200248g>.
- 508 (17) Sava, D. F.; Rodriguez, M. A.; Chapman, K. W.; Chupas, P. J.; Greathouse, J. A.; Crozier, P. S.;
509 Nenoff, T. M. Capture of Volatile Iodine, a Gaseous Fission Product, by Zeolitic Imidazolate

510 Framework-8. *J. Am. Chem. Soc.* **2011**, 133 (32), 12398–12401.
511 <https://doi.org/10.1021/ja204757x>.

512 (18) Riley, B. J.; Vienna, J. D.; Strachan, D. M.; McCloy, J. S.; Jerden, J. L. Materials and Processes for
513 the Effective Capture and Immobilization of Radioiodine: A Review. *J. Nucl. Mater.* **2016**, 470,
514 307–326. <https://doi.org/10.1016/j.jnucmat.2015.11.038>.

515 (19) Frankel, G. S.; Vienna, J. D.; Lian, J.; Scully, J. R.; Gin, S.; Ryan, J. V.; Wang, J.; Kim, S. H.; Windl, W.;
516 Du, J. A Comparative Review of the Aqueous Corrosion of Glasses, Crystalline Ceramics, and
517 Metals. *npj Materials Degradation* **2018**, 2 (1), 15. <https://doi.org/10.1038/s41529-018-0037-2>.

518 (20) Faucon, P.; Adenot, F.; Jacquinet, J. F.; Petit, J. C.; Cabrillac, R.; Jorda, M. Long-Term Behaviour of
519 Cement Pastes Used for Nuclear Waste Disposal: Review of Physico-Chemical Mechanisms of
520 Water Degradation. *Cem. Concr. Res.* **1998**, 28 (6), 847–857. [https://doi.org/10.1016/S0008-](https://doi.org/10.1016/S0008-8846(98)00053-2)
521 [8846\(98\)00053-2](https://doi.org/10.1016/S0008-8846(98)00053-2).

522 (21) Frankel, G. S.; Vienna, J.; Lian, J. WastePD, an Innovative Center on Materials Degradation. *npj*
523 *Mater. Degrad.* **2017**, 1 (1), 5. <https://doi.org/10.1038/s41529-017-0002-5>.

524 (22) Chapman, N. A.; McKinley, I. G.; Smellie, J. a. T. The Potential of Natural Analogues in Assessing
525 Systems for Deep Disposal of High-Level Radioactive Waste; EIR--545; Eidgenossisches Inst. fuer
526 Reaktorforschung: Sweden, 1984.

527 (23) Kato, H.; Kato, O.; Tanabe, H. Review of Immobilization Techniques of Radioactive Iodine for
528 Geological Disposal. **2002**. <https://doi.org/10.11484/JAERI-Conf-2002-004>.

529 (24) Chapman, K. W.; Chupas, P. J.; Nenoff, T. M. Radioactive Iodine Capture in Silver-Containing
530 Mordenites through Nanoscale Silver Iodide Formation. *J. Am. Chem. Soc.* **2010**, 132 (26), 8897–
531 8899. <https://doi.org/10.1021/ja103110y>.

532 (25) Yao, T.; Lu, F.; Sun, H.; Wang, J.; Ewing, R. C.; Lian, J. Bulk Iodoapatite Ceramic Densified by Spark
533 Plasma Sintering with Exceptional Thermal Stability. *J. Am. Ceram. Soc.* **2014**, 97 (8), 2409–2412.
534 <https://doi.org/10.1111/jace.13101>.

535 (26) Maddrell, E.; Gandy, A.; Stennett, M. The Durability of Iodide Sodalite. *Journal of Nuclear*
536 *Materials* **2014**, 449 (1), 168–172. <https://doi.org/10.1016/j.jnucmat.2014.03.016>.

537 (27) Chong, S.; Peterson, J. A.; Riley, B. J.; Tabada, D.; Wall, D.; Corkhill, C. L.; McCloy, J. S. Glass-
538 Bonded Iodosodalite Waste Form for Immobilization of ¹²⁹I. *J. Nucl. Mater.* **2018**, 504, 109–121.
539 <https://doi.org/10.1016/j.jnucmat.2018.03.033>.

540 (28) Le Gallet, S.; Campayo, L.; Courtois, E.; Hoffmann, S.; Grin, Yu.; Bernard, F.; Bart, F. Spark Plasma
541 Sintering of Iodine-Bearing Apatite. *J. Nucl. Mater.* **2010**, 400 (3), 251–256.
542 <https://doi.org/10.1016/j.jnucmat.2010.03.011>.

543 (29) Zhang, Z.; Heath, A.; T. Valsaraj, K.; L. Ebert, W.; Yao, T.; Lian, J.; Wang, J. Mechanism of Iodine
544 Release from Iodoapatite in Aqueous Solution. *RSC Adv.* **2018**, 8 (8), 3951–3957.
545 <https://doi.org/10.1039/C7RA11049A>.

546 (30) Gauthier-Lafaye, F. 2 Billion Year Old Natural Analogs for Nuclear Waste Disposal: The Natural
547 Nuclear Fission Reactors in Gabon (Africa). *C. R. Phys.* **2002**, 3 (7), 839–849.
548 [https://doi.org/10.1016/S1631-0705\(02\)01351-8](https://doi.org/10.1016/S1631-0705(02)01351-8).

549 (31) Uno, M.; Shinohara, M.; Kurosaki, K.; Yamanaka, S. Some Properties of a Lead Vanado-
550 Iodoapatite Pb₁₀(VO₄)₆I₂. *J. Nucl. Mater.* **2001**, 294 (1), 119–122.
551 [https://doi.org/10.1016/S0022-3115\(01\)00462-7](https://doi.org/10.1016/S0022-3115(01)00462-7).

552 (32) National Research Council. Scho; 2011. <https://doi.org/10.17226/13100>.

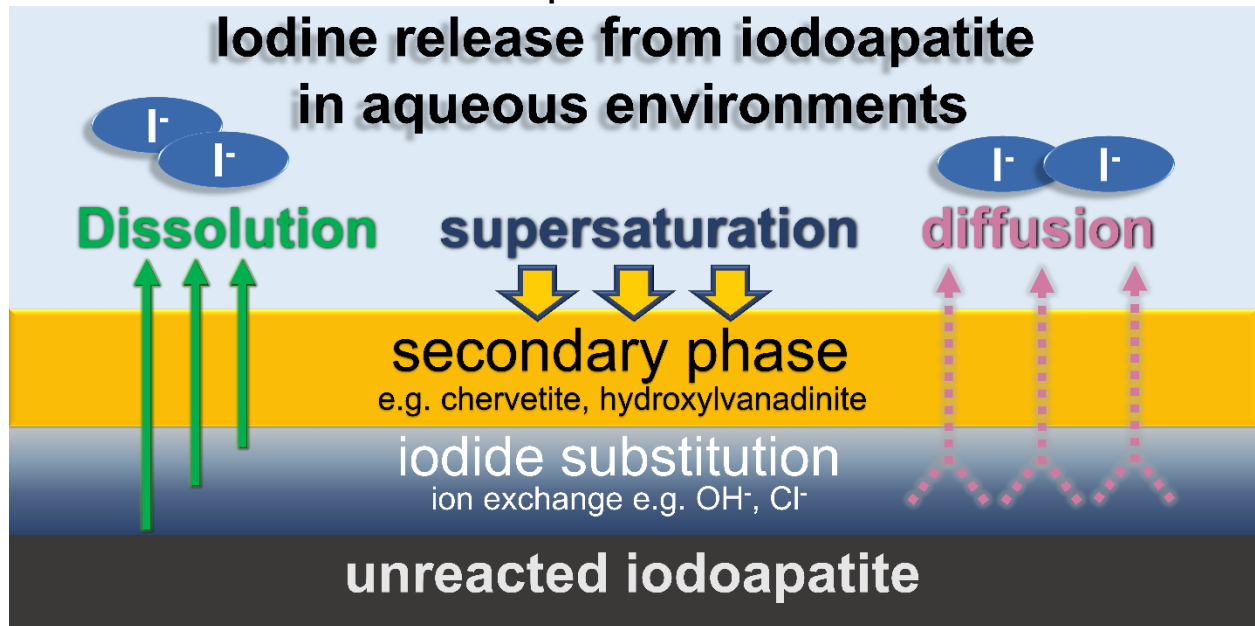
553 (33) Guy, C.; Audubert, F.; Lartigue, J.-E.; Latrille, C.; Advocat, T.; Fillet, C. New Conditionings for
554 Separated Long-Lived Radionuclides. *C. R. Phys.* **2002**, 3 (7), 827–837.
555 [https://doi.org/10.1016/S1631-0705\(02\)01377-4](https://doi.org/10.1016/S1631-0705(02)01377-4).

- 556 (34) Zhang, M.; Maddrell, E. R.; Abraitis, P. K.; Salje, E. K. H. Impact of Leach on Lead Vanado-
557 Iodoapatite [Pb₅(VO₄)₃I]: An Infrared and Raman Spectroscopic Study. *Mater. Sci. Eng. B* **2007**,
558 137 (1), 149–155. <https://doi.org/10.1016/j.mseb.2006.11.003>.
- 559 (35) Coulon, A.; Grandjean, A.; Laurencin, D.; Jollivet, P.; Rossignol, S.; Campayo, L. Durability Testing
560 of an Iodate-Substituted Hydroxyapatite Designed for the Conditioning of 129I. *J. Nucl. Mater.*
561 **2017**, 484, 324–331. <https://doi.org/10.1016/j.jnucmat.2016.10.047>.
- 562 (36) ASTM C1220-17, Standard Test Method for Static Leaching of Monolithic Waste Forms for
563 Disposal of Radioactive Waste; ASTM International: West Conshohocken, PA, 2017.
- 564 (37) Zhang, Z.; Ebert, W. L.; Yao, T.; Lian, J.; Valsaraj, K. T.; Wang, J. Chemical Durability and
565 Dissolution Kinetics of Iodoapatite in Aqueous Solutions. *ACS Earth Space Chem.* **2019**, 3 (3), 452-
566 462. <https://doi.org/10.1021/acsearthspacechem.8b00162>.
- 567 (38) Zhu, Y.; Zhang, X.; Chen, Y.; Xie, Q.; Lan, J.; Qian, M.; He, N. A Comparative Study on the
568 Dissolution and Solubility of Hydroxylapatite and Fluorapatite at 25°C and 45°C. *Chem. Geol.*
569 **2009**, 268 (1), 89–96. <https://doi.org/10.1016/j.chemgeo.2009.07.014>.
- 570 (39) Cazalbou, S.; Eichert, D.; Ranz, X.; Drouet, C.; Combes, C.; Harmand, M. F.; Rey, C. Ion Exchanges
571 in Apatites for Biomedical Application. *J. Mater. Sci. Mater. Med.* **2005**, 16 (5), 405–409.
572 <https://doi.org/10.1007/s10856-005-6979-2>.
- 573 (40) Brenan, J. Kinetics of Fluorine, Chlorine and Hydroxyl Exchange in Fluorapatite. *Chem. Geol.* **1993**,
574 110 (1), 195–210. [https://doi.org/10.1016/0009-2541\(93\)90254-G](https://doi.org/10.1016/0009-2541(93)90254-G).
- 575 (41) Dorozhkin, S. V. A Review on the Dissolution Models of Calcium Apatites. *Prog. Cryst. Growth*
576 *Charact.* **2002**, 44 (1), 45–61. [https://doi.org/10.1016/S0960-8974\(02\)00004-9](https://doi.org/10.1016/S0960-8974(02)00004-9).
- 577 (42) Petříček, V.; Dušek, M.; Palatinus, L. Crystallographic Computing System JANA2006: General
578 Features. *Z. Kristallogr. Cryst. Mater.* **2014**, 229 (5), 345–352. <https://doi.org/10.1515/zkri-2014-1737>.
- 580 (43) Audubert, F.; Savariault, J.-M.; Lacout, J.-L. Pentalead Tris(Vanadate) Iodide, a Defect Vanadinite-
581 Type Compound. *Acta Crystallogr. C* **1999**, 55 (3), 271–273.
582 <https://doi.org/10.1107/S0108270198005034>.
- 583 (44) Ślósarczyk, A.; Paszkiewicz, Z.; Paluszkiwicz, C. FTIR and XRD Evaluation of Carbonated
584 Hydroxyapatite Powders Synthesized by Wet Methods. *J. Mol. Struct.* **2005**, 744–747, 657–661.
585 <https://doi.org/10.1016/j.molstruc.2004.11.078>.
- 586 (45) Merry, J. C.; Gibson, I. R.; Best, S. M.; Bonfield, W. Synthesis and Characterization of Carbonate
587 Hydroxyapatite. *J. Mater. Sci. Mater. Med.* **1998**, 9 (12), 779–783.
588 <https://doi.org/10.1023/A:1008975507498>.
- 589 (46) Roobottom, H. K.; Jenkins, H. D. B.; Passmore, J.; Glasser, L. Thermochemical Radii of Complex
590 Ions. *J. Chem. Educ.* **1999**, 76 (11), 1570. <https://doi.org/10.1021/ed076p1570>.
- 591 (47) Guidry, M. W.; Mackenzie, F. T. Experimental Study of Igneous and Sedimentary Apatite
592 Dissolution: Control of PH, Distance from Equilibrium, and Temperature on Dissolution Rates.
593 *Geochim. Cosmochim. Acta* **2003**, 67 (16), 2949–2963. [https://doi.org/10.1016/S0016-7037\(03\)00265-5](https://doi.org/10.1016/S0016-7037(03)00265-5).
- 595 (48) Cao, C.; Chong, S.; Thirion, L.; C. Mauro, J.; S. McCloy, J.; Goel, A. Wet Chemical Synthesis of
596 Apatite-Based Waste Forms – A Novel Room Temperature Method for the Immobilization of
597 Radioactive Iodine. *J. Mater. Chem. C* **2017**, 5 (27), 14331–14342.
598 <https://doi.org/10.1039/C7TA00230K>.
- 599 (49) Campayo, L.; Audubert, F.; Lartigue, J.-E.; Courtois-Manara, E.; Gallet, S. L.; Bernard, F.; Lemesle,
600 T.; Mear, F. O.; Montagne, L.; Coulon, A.; et al. French Studies on the Development of Potential
601 Conditioning Matrices for Iodine 129. *Mater. Res. Soc. Symp. Proc.* **2015**, 1744, 15–20.
602 <https://doi.org/10.1557/opl.2015.309>.

- 603 (50) Zapanta-Legeros, R. Effect of Carbonate on the Lattice Parameters of Apatite. *Nature* **1965**, 206
604 (4982), 403. <https://doi.org/10.1038/206403a0>.
- 605 (51) White, T. J.; Dong, Z. L. Structural Derivation and Crystal Chemistry of Apatites. *Acta Cryst. B*
606 **2003**, 59 (1), 1–16. <https://doi.org/10.1107/S0108768102019894>.
- 607 (52) Fleet, M. E.; Liu, X. Coupled Substitution of Type A and B Carbonate in Sodium-Bearing Apatite.
608 *Biomaterials* **2007**, 28 (6), 916–926. <https://doi.org/10.1016/j.biomaterials.2006.11.003>.
- 609 (53) Landi, E.; Tampieri, A.; Celotti, G.; Vichi, L.; Sandri, M. Influence of Synthesis and Sintering
610 Parameters on the Characteristics of Carbonate Apatite. *Biomaterials* **2004**, 25 (10), 1763–1770.
611 <https://doi.org/10.1016/j.biomaterials.2003.08.026>.
612

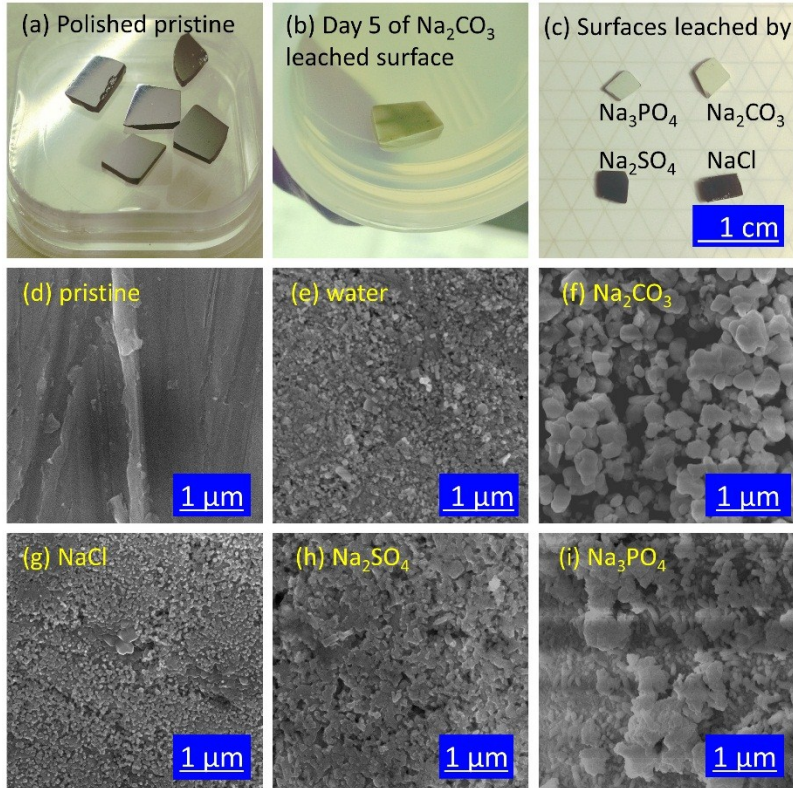
613

Graphical abstract



614

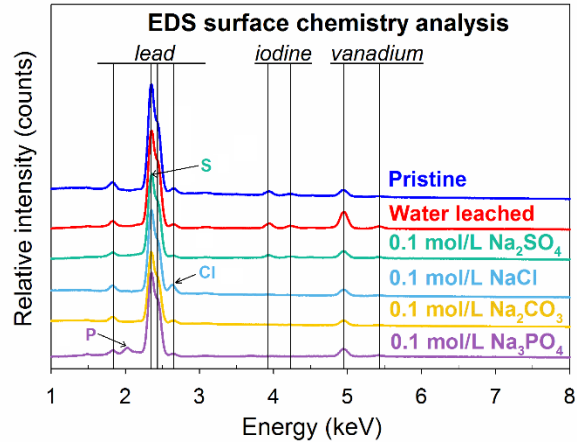
615



616

617 Fig. 1.(a) Polished pristine iodoapatite samples before test, (b) iodoapatite leached
 618 surface during the 5th replacement of Na_2CO_3 solution, (c) surface leached by at the end
 619 of 14-day leaching tests, SEM images of (a) a polished pristine iodoapatite and the
 620 samples leached by (b) deionized water, (c) 0.1 mol/L Na_2CO_3 , (d) 0.1 mol/L NaCl , (e)
 621 0.1 mol/L Na_2SO_4 , and (f) 0.1 mol/L Na_3PO_4 .

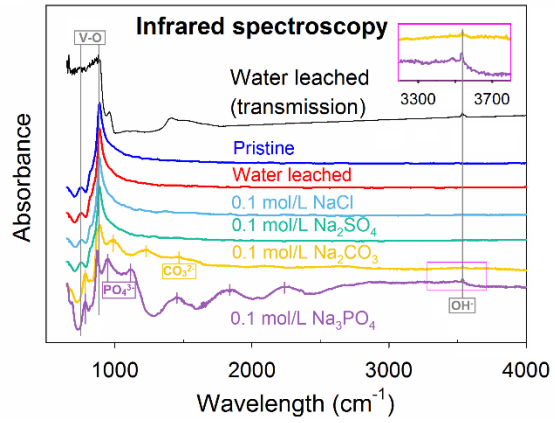
622



623

624 Fig. 2. EDS spectra of a pristine iodoapatite and the samples leached by deionized
 625 water, 0.1 mol/L NaCl, 0.1 mol/L Na₂CO₃, 0.1 mol/L Na₃PO₄, and 0.1 mol/L Na₂SO₄
 626 solutions.

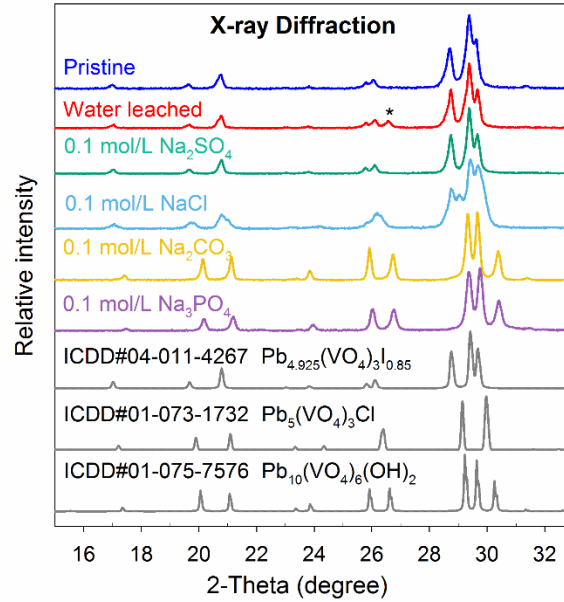
627



628

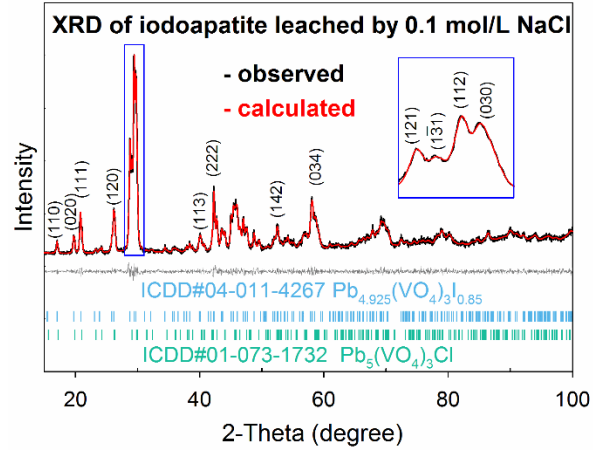
629 Fig. 3. Infrared spectroscopy of pristine iodoapatite and leached samples by deionized
630 water, NaCl, Na₂SO₄, Na₂CO₃, and Na₃PO₄ solutions.

631



632

633 Fig. 4. XRD patterns of a pristine iodoapatite and the samples leached by deionized
 634 water, 0.1 mol/L Na₂SO₄, 0.1 mol/L NaCl, 0.1 mol/L Na₂CO₃, and 0.1 mol/L Na₃PO₄. In
 635 addition, standard XRD spectra of iodoapatite, vanadinite, and hydroxylvanadinite are
 636 listed for comparison. * denotes the graphite impurity introduced during sample
 637 synthesis.²⁵

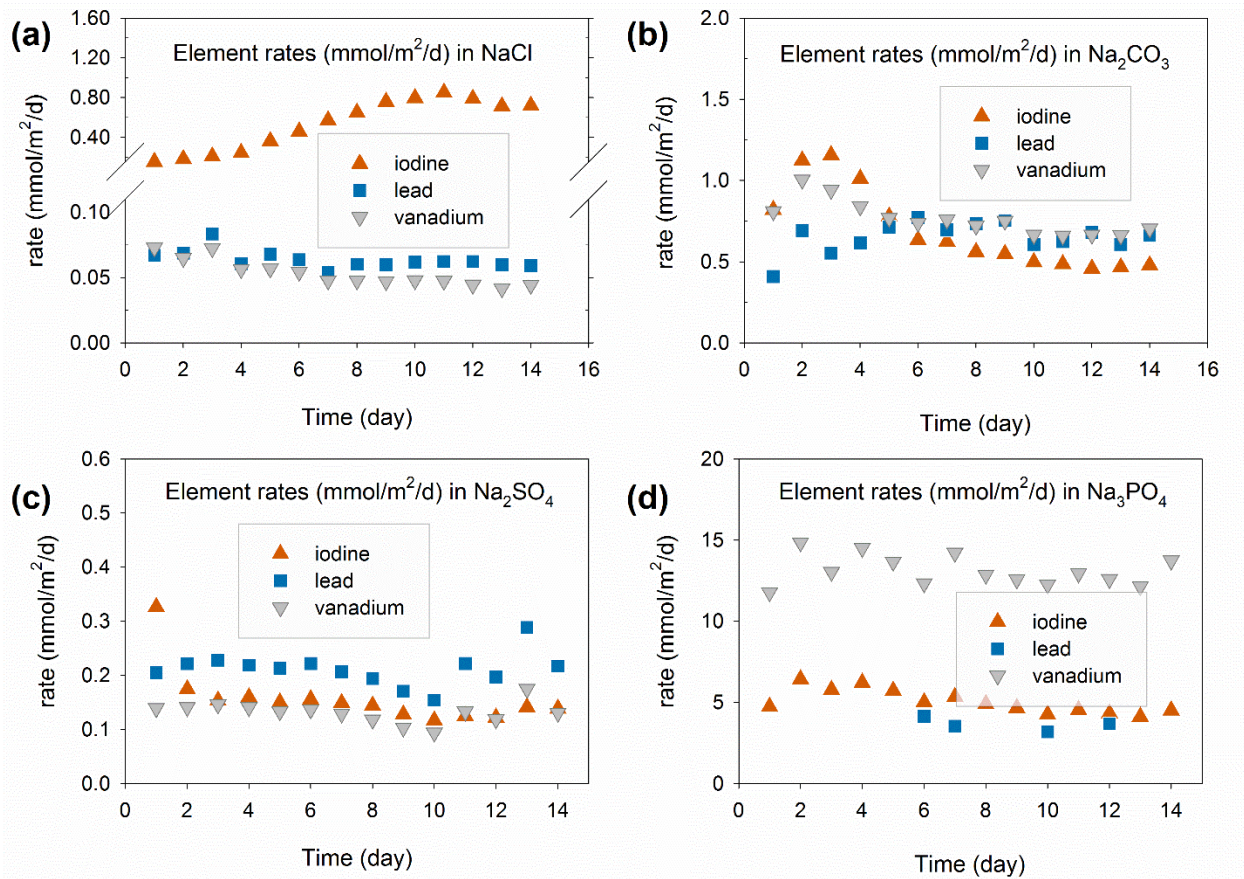


638

639 Fig. 5. XRD phase analysis of the iodoapatite sample surface leached by 0.1
640 mol/L NaCl solution. Two phases were identified: iodoapatite and vanadinite.

641

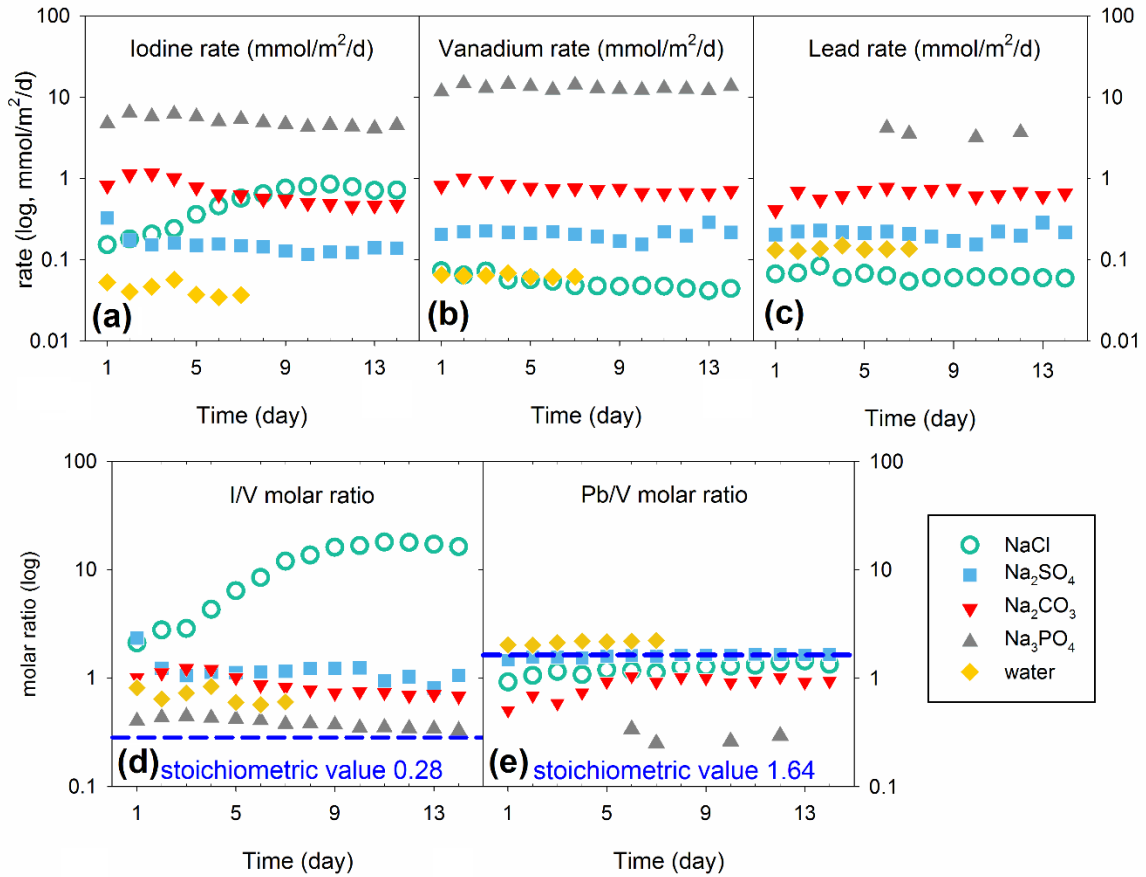
642



643

644 Fig. 6. Solution analysis of collected leachates from 14 days semi-dynamic leach tests
645 on iodoapatite samples in (a) 0.1 mol/L NaCl, (b) 0.1 mol/L Na₂CO₃, (c) 0.1 mol/L
646 Na₂SO₄, and (d) 0.1 mol/L Na₃PO₄.

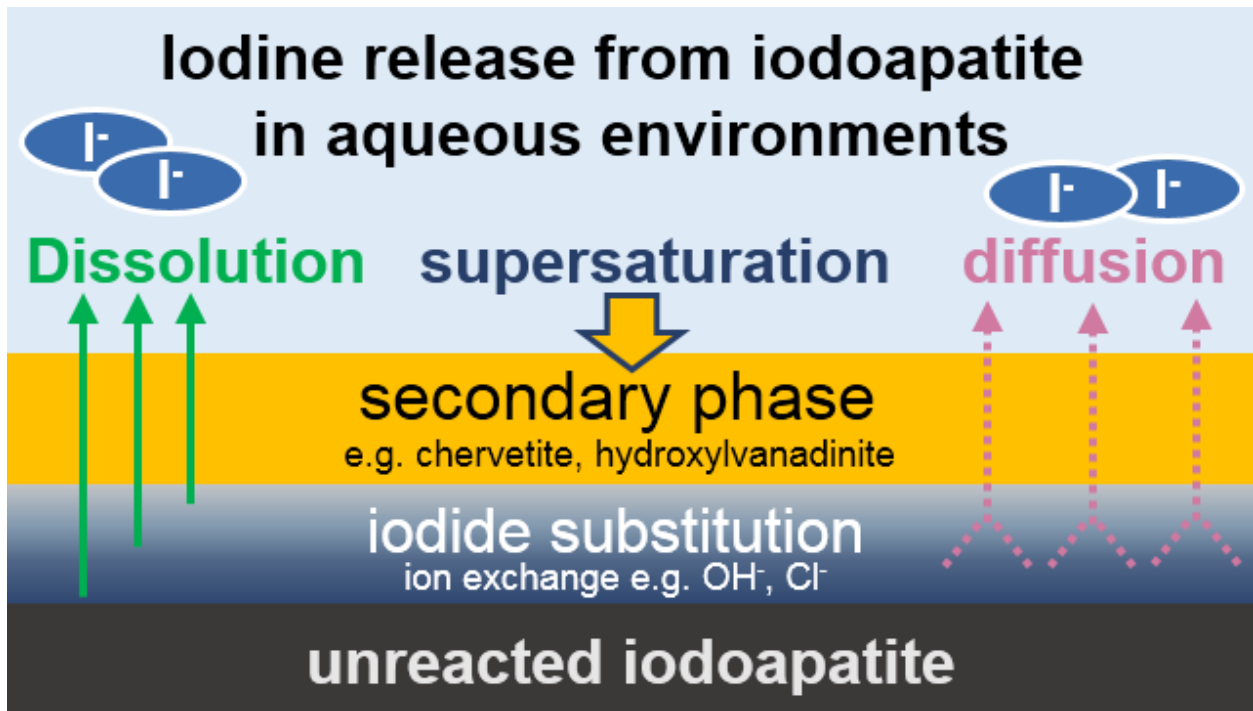
647



648

649 Fig. 7. Comparison of element release rate of iodine (a), vanadium (b), and lead (c) in
 650 the leachate solutions from different leach tests. Molar ratios of Pb/V (d) and I/V (e) in
 651 leachate solutions from leach tests in NaCl, Na₂SO₄, Na₂CO₃, Na₃PO₄, and deionized
 652 water.

653



654

655 Fig. 8. Schematic diagram illustrates major processes that control the iodine release
 656 from iodoapatite in aqueous environments

657 Table. 1 Crystallographic parameters based on the XRD refinements by Le Bail
 658 algorithm.

Leach test condition	Refined parameters				
	a, b (a=b, Å)	c (Å)	GoF	R _p (%)	R _{wp} (%)
Pristine	10.4420 (3)	7.4756 (3)	1.32	5.16	6.53
Water	10.4325 (3)	7.4864 (3)	1.63	6.04	7.73
0.1 mol/L Na ₂ SO ₄	10.4336 (2)	7.4837 (2)	1.39	4.60	5.93
0.1 mol/L Na ₂ CO ₃	10.1923 (2)	7.4656 (2)	1.65	4.85	6.44
0.1 mol/L Na ₃ PO ₄	10.1984 (2)	7.4449 (2)	1.43	4.74	6.23
0.1 mol/L NaCl (2 phases)	10.4443 (6)	7.4796 (5)	1.17	4.12	5.28
	10.3536 (8)	7.3735(8)			
Pb_{4.925}(VO₄)₃l_{0.85} [ICDD#04-011-4267]	10.422	7.467	Crystal system: hexagonal		
Pb₅(VO₄)₃(OH) [ICDD#01-075-7576]	10.2242	7.4537	Space group: P63/m #176;		
Pb₅(VO₄)₃Cl [ICDD#01-073-1732]	10.31	7.34	α=90° β=90° γ=120°		

659

660

661 Table 2. Solution chemistry at equilibrium state calculated by Visual MINTEQ under
 662 90 °C.

mol/L 90 °C	Deionized water	0.1 mol/L NaCl	0.1 mol/L Na ₂ SO ₄	0.1 mol/L Na ₂ CO ₃	0.1 mol/L Na ₃ PO ₄
pH (unitless)	6.1	6.1	6.2	10.3	10.9
Ionic strength	2.04×10^{-6}	0.098	0.26	0.25	0.29
Major cation	H⁺	Na⁺	Na⁺	Na⁺	Na⁺
Concentration	6.52×10^{-7}	0.098	0.18	0.18	0.22
Activity	6.51×10^{-7}	0.074	0.13	0.13	0.15
Activity coefficient	1.00	0.76	0.72	0.72	0.68
Major anion	OH⁻	Cl⁻	SO₄²⁻	CO₃²⁻	PO₄³⁻
Concentration	8.72×10^{-7}	0.098	0.079	0.069	0.012
Activity	8.70×10^{-7}	0.074	0.02	0.017	0.00049
Activity coefficient	1.00	0.76	0.25	0.24	0.041

663